Su *et al. Sustainable Environment Research* (2022) 32:27
https://doi.org/10.1186/s42834-022-00138-7

Sustainable Environment Research

RESEARCH Open Access

# Chitosan@$TiO_2$ composites for the adsorption of copper(II) and antibacterial applications

Chien Su[1], Abiyu Kerebo Berekute[1,2] and Kuo-Pin Yu[1,2*]

**Abstract**

Chitosan (CS) is a biopolymer that is well known for its ubiquity, biodegradability, lack of toxicity, low cost, antibacterial activity, and excellent heavy metal adsorption ability. We synthesized CS and CS@$TiO_2$ composites (CST) with different concentrations of glutaraldehyde (crosslinking agent) solution by a simple method involving a crosslinking process (using glutaraldehyde as the crosslinking agent), a freeze-drying technique, and exchange with ammonia solution. The interaction mechanisms of the as-synthesized samples were systematically characterized by scanning electron microscopy, electron dispersive X-ray spectroscopy, Fourier transform infrared spectroscopy, thermogravimetric analysis, and the Brunauer-Emmett-Teller method. Among the as-synthesized samples, 3%CS-V (CS composites synthesized using 3% glutaraldehyde for crosslinking and exchanged with ammonia solution) at an initial concentration of 300 ppm exhibited a preferable adsorption capacity for copper ions ($Cu^{2+}$), with a maximum adsorption capacity of 31 mg $g^{-1}$. Sorption equilibrium isotherms fit the Freundlich model. Compared to CS, 7%CST-V (CST composite synthesized using 7% glutaraldehyde for crosslinking and exchanged with ammonia solution) exhibited higher antibacterial activity against *Staphylococcus epidermidis* due to a synergistic effect. The antimicrobial efficacy against *Escherichia coli* was more affected by copper ions than $TiO_2$ addition and glutaraldehyde concentration, whereas the antimicrobial efficacy against *S. epidermidis* was more affected by $TiO_2$ addition and exchange with ammonia solution.

**Keywords:** Adsorption, Chitosan@$TiO_2$, Copper ion, Antibacterial application

## 1 Introduction

Heavy metals are major environmental pollutants due to their toxicity, persistence, and bioaccumulation in environmental matrices, and they pose a serious threat to living organisms. Copper ions ($Cu^{2+}$) have been selected as the target pollutant because they are a principal constituent in the wastewater of the printed circuit board (PCB) industry [1, 2]. In this regard, finding a sustainable solution to reduce heavy metal pollution has become a major environmental issue. Therefore, various conventional techniques have been developed to remove heavy metals from industrial effluents, such as chemical precipitation, membrane filtration, ion exchange, sedimentation, and adsorption [3]. Among these, adsorption is a promising technique for removing heavy metals from aqueous solution due to its low cost, simplicity, efficiency, and eco-friendliness [4].

Adsorbent materials based on chitosan (CS) biopolymers have proven to favor the adsorption of heavy metals from wastewater. CS is a versatile hydrophilic polysaccharide produced from the partial deacetylation of chitin that is usually obtained from shells of shrimp or other shellfish and consists of β-(1–4) glycosidic links, 2-amino− 2-deoxy-D-glucan, and 2-acetamidodeoxy-D-glucan [5]. The presence of amine ethane

*Correspondence: kpyu03@nycu.edu.tw

[2] International Ph.D. Program in Environmental Science and Technology, National Yang Ming Chiao Tung University, Taipei 112304, Taiwan
Full list of author information is available at the end of the article

© The Author(s) 2022. **Open Access** This article is licensed under a Creative Commons Attribution 4.0 International License, which permits use, sharing, adaptation, distribution and reproduction in any medium or format, as long as you give appropriate credit to the original author(s) and the source, provide a link to the Creative Commons licence, and indicate if changes were made. The images or other third party material in this article are included in the article's Creative Commons licence, unless indicated otherwise in a credit line to the material. If material is not included in the article's Creative Commons licence and your intended use is not permitted by statutory regulation or exceeds the permitted use, you will need to obtain permission directly from the copyright holder. To view a copy of this licence, visit http://creativecommons.org/licenses/by/4.0/.

($-NHCOCH_3$), hydroxy ($-OH$), and amine ($-NH_2$) groups that are easily functionalized in the chitosan polymer and the hydrophilicity of CS make it attractive for use in multiple applications, such as biomedicine, agriculture, and wastewater treatments [6, 7]. The amine groups on CS chains serve as coordination sites, thereby playing an important role in the adsorption capacity of CS [8, 9].

CS is a biopolymer well known for its ubiquity, biodegradability, natural abundance, biocompatibility, nontoxicity, low cost, antibacterial ability, and excellent capacity for heavy metal adsorption [5]. It can adsorb transition metals via several mechanisms, including chemical interactions (chelation or complexation), ion exchange, electrostatic attractions, and nonpolar interactions, such as van der Waals forces, thus demonstrating its potential for recycling heavy metals. The removal of heavy metals with CS-based composites has been studied by various researchers. For example, Chen and Wang [7] reported that the $Fe_2O_3$@CS composite was effective for removing $Cu^{2+}$ from water. The adsorption capacity for $Cu^{2+}$ was 35.5 mg $g^{-1}$. Wang and Kuo reported that CS@poly(acrylic acid) nanoparticles effectively adsorb nickel ions. The adsorption capacity for $Ni^{2+}$ was 435 mg $g^{-1}$ [10]. In addition, Peralta et al. [11] reported the adsorption of heavy metal ions on magnetic CS composites. The adsorption capacities for $Cu^{2+}$, $Pb^{2+}$ and $Ni^{2+}$ were 217, 221 and 109 mg $g^{-1}$, respectively.

Furthermore, chitosan has long been noted for its antibacterial activity. According to Goy et al. [12], three antimicrobial mechanisms of CS have been suggested. These include the interaction between positively charged CS molecules and negatively charged microbial cell membranes, the binding of CS with microbial DNA, and the chelation of metals.

Similar to CS, $TiO_2$ and copper also have antimicrobial properties. During the past few decades, titanium dioxide has been one of the most important and widely used compounds in all application areas, including its use in building materials, biomedical applications, photocatalysts, paints/coatings, and sunscreens due to its strong oxidizability, chemical inertness, antimicrobial ability, and nontoxicity [13].

The mechanism of killing Gram-positive and Gram-negative bacteria using $TiO_2$ has been extensively studied. Some evidence, including microscopic images, the detection of lipid peroxidation products, and the leakage of intracellular components, has proven that the lethality of $TiO_2$ is due to cell membrane and cell wall damage [14]. Another study indicated that $TiO_2$ could produce reactive oxygen species (ROS), which can result in the depletion of antioxidants leading to oxidative stress and can damage the cell membrane [15].

Recently, nanometals have been widely used as antimicrobial agents. Among metallic substances, silver and copper are usually studied since they have excellent antimicrobial efficiencies. Zhao and Stevens [16] investigated metal toxicity related to microorganisms. Accordingly, they found that the most toxic metals for microorganisms were in the order Ag > Hg > Cu > Cr > Pb > Co > Au > Zn > Fe > Mn > Mo > Sn. According to the Integrated Risk Information System of the USEPA, the health risk of antimicrobial metals for humans is in the order $Cr^{6+}$ > Hg > Ag > Cu. Thus, the study indicated that Ag and Cu have the highest potential for antimicrobial applications. The antibacterial mechanisms of copper have been associated with multiple toxicities, such as the production of ROS and reactive hydroxyl radicals through the Fenton reaction, which causes oxidative damage to the cell membrane and DNA degradation in *Escherichia coli* cells [17].

Koyama and Taniguchi [17] reported the adsorption capability of CS and cross-linked CS for Cu. This result showed that an aldehyde-amino group ratio of approximately 0.7 had better capability. This was most likely because of the accessibility of chelating groups as a result of the partial destruction of the crystalline structure by crosslinking with glutaraldehyde. Glutaraldehyde has antimicrobial and cytotoxic effects, the mean antimicrobial concentration of glutaraldehyde was 1.418%, which can kill *Staphylococcus epidermidis*, and the cytotoxic potential of glutaraldehyde was less than that of formocresol [18]. Therefore, this study used glutaraldehyde as the crosslinking agent for the synthesis of CS and CS@$TiO_2$ (CST) composites.

In this study, we synthesized CS and CST composites with different concentrations of glutaraldehyde solution by a simple method involving a crosslinking process and freeze-drying technique. The present study aims to optimize the performance of CS and CST composites for copper ion adsorption and to evaluate the effectiveness of chitosan composites after absorption copper against *S. epidermidis* and *E. coli*. Subsequently, we compared the absorbent efficiencies and antimicrobial efficacies of CS and CST composites. The interaction mechanisms of the as-synthesized samples were systematically characterized by scanning electron microscopy (SEM), Fourier transform infrared (FT-IR) spectroscopy, the Brunauer-Emmett-Teller (BET) method, and thermogravimetric analysis (TGA).

## 2 Materials and methods

### 2.1 Materials

#### *2.1.1 Chemicals*

CS (90%; First Chemical Co.), titanium dioxide (Degussa P25 $TiO_2$; 80%; Evonik Industries), copper(II) nitrate,

2.5-hydrate (99%; JT Baker), ammonium chloride (≥ 99.5%; Fluka™), ammonium hydroxide solution (~25% $NH_3$ basis; Fluka™), tryptone soya agar (TSA; Oxoid™), ammonia solution (2 M in ethanol; Sigma-Aldrich), bis(cyclohexanone) oxaldihydrazone (for the spectrophotometric det. of Cu, ≥ 99.0%; Sigma-Aldrich), nitric acid (60%; Merck), sodium hydroxide (NaOH; First Chemical Co.), acetic acid ($CH_3COOH$; assay: ≥ 99.7%; JT Baker), glutaraldehyde solution (Grade 1, 25% in $H_2O$; Sigma-Aldrich), glutaraldehyde solution (2.5%; First Chemical Co.) and lysogeny broth (LB) (Miller, Difco™) were all purchased and used as received without further purification. Deionized water was used in all experiments.

#### *2.1.2 Synthesis of CS and CST composites*

The CST composites were synthesized with some modification according to a method in the literature [19]. Initially, 1 g of chitosan was dissolved at room temperature in 90 mL of 3% (v/v) acetic acid solution (pH = 2.6) and stirred continuously. After CS was evenly mixed in the acetic acid solution, 1.6 g of $TiO_2$ Degussa P25 powder was dispersed in the CS solution, and both the CS solution and CS/$TiO_2$ mixture were added to 10 mL of glutaraldehyde solution (as a crosslinking agent at concentrations of 3, 5, and 7% w/w) as the solution was vigorously stirred for 10 min. Then, the viscous solution was poured into a test tube and used as a template, and the test tubes were put into a test tube rack for a 10 min ultrasonic treatment to remove the bubbles. The viscous solution in molds was covered with aluminum foil to prevent exposure to visible light, and the crosslinked hydrogels were kept for 45 h at room temperature. The tawny CS hydrogel and the opalescent CST hydrogel were then frozen at −68 °C for 2 h. This was followed by exchanging half of the solvent with 0.5 M ammonia solution for 30 min. The sample was then rinsed several times with deionized water until its pH became neutral. Finally, all of the composites were obtained without exposure to visible light after freeze-drying for 48 h. All these samples were marked α%CS-V(X) and α%CST-V(X), where α was the concentration of glutaraldehyde solution (3, 5, 7) and V and X represented whether the composites were exchanged with the ammonia solution. The process used for the as-synthesized composites is shown in Fig. S1 in Supplemental Materials.

#### *2.1.3 Characterization of composites*

The surface of the composites and the elemental compositions were studied by field-emission SEM (FE-SEM; JEOL JSM-7600F, Tokyo, Japan) equipped with energy dispersive spectroscopy (EDS) performed at an accelerating voltage of 15 kV. The BET surface area ($S_{BET}$) of the samples was acquired from nitrogen adsorption data recorded on a gas volumetric analyzer (Quantachrome AutoIQ, USA). All samples were degassed at 120 °C before the nitrogen adsorption measurements. FT-IR spectra (4200 FT-IR spectrometer, Jasco) were obtained to determine the chemical bonding of the as-synthesized samples. TGA (TA Q50, DuPont) was performed to evaluate the thermal stability of the as-synthesized samples.

### 2.2 Batch adsorption experiments

The effects of adding $TiO_2$, the degree of crosslinking, and the execution of the ammonia treatment on the adsorption of copper ions were tested using the following steps [19]: Each sample of approximately 50 mg was put into a 250 mL beaker containing 50 mL of different concentrations of copper nitrate solution for 12 h at room temperature. (Initially, the batch adsorption experiments continued for 24 h. However, we found that the 24-h adsorption results were almost the same as the 12-h adsorption results. Therefore, the adsorption equilibrium time for copper ions was set to 12 h based on the test results.) The sample was shaken at 150 rpm; furthermore, the beaker was covered with aluminum foil to prevent exposure to light. To adjust the copper nitrate solution to a pH of 6.0, 0.1 M NaOH solution was added beforehand. The ion concentration of Cu was then determined using the spectrophotometry-BCO method, using bis(cyclohexanone) oxaldihydrazone (BCO) as an indicator. Preliminarily, 5 mL of BCO solution (1 g dissolved in 500 mL of deionized water), 10 mL of $NH_3$-$NH_4Cl$ buffer solution (35 g of $NH_4Cl$ and 24 mL of $NH_3 \cdot H_2O$ dissolved in 500 mL of deionized water) and 200 µL of sample solution were mixed in an Erlenmeyer flask, and the solution was then diluted with 50 mL of deionized water. After 10 min, the absorbance at 602 nm was measured, and a standard calibration curve was created for each experiment to determine the Cu concentration. The adsorption capacity ($q_e$, mg $g^{-1}$) was calculated according to the following formula:

$$q_e = \frac{(C_0 - C_e) \times V}{m_0} \tag{1}$$

where $C_0$ (mg $L^{-1}$) and $C_e$ represent the concentration of $Cu^{2+}$ at the initial time and the 12th h, respectively, V is the volume of the $Cu^{2+}$ solution, and $m_0$ is the mass of the CS or CST samples added to the $Cu^{2+}$ solution before adsorption.

The adsorption data of the CS and CST composite samples were arranged using the Freundlich isotherm model:

$$\ln q_e = \ln K_F + \frac{1}{n} \times \ln C_e \tag{2}$$

where $q_e$ is the amount absorbed ($mg\,g^{-1}$) at equilibrium and $C_e$ is the equilibrium concentration of copper ions in solution ($mg\,L^{-1}$). $K_F$ and $n$ are the Freundlich model constants, indicating the capacity and intensity of adsorption, respectively [19].

### 2.3 Microbial cultures

Microbial cultures of *E. coli* [Bioresource Collection and Research Center, (BCRC) 50,354] and *S. epidermidis* (BCRC 11030) were obtained from the BCRC of Taiwan in freeze-dried form for use in antimicrobial experiments. Before their use in this study, the bacterial strains were prepared by following the instruction guide from the BCRC using TSA and LB as cultivation media. To prepare the bacterial suspensions, a single colony of each bacterial strain was inoculated into 10 mL of LB medium with an inoculating loop. The cultures were incubated at 37 °C with a shaking rate of 50–100 rpm for 16–18 h. The final bacterial concentration was approximately $1.7 \times 10^6\,CFU\,mL^{-1}$.

### 2.4 Evaluation of antibacterial activity

The zone of inhibition (ZOI) assay was used to evaluate the antimicrobial efficacy [20]. The experimental process is shown in Fig. S2. First, 500 µL of the microbial suspension ($10^6$–$10^7\,CFU\,mL^{-1}$) was evenly spread on a TSA plate. After adsorption of copper ions, the CS and CST composites were placed on the surface of the agar plates inoculated with test microbes. These agar plates were incubated under suitable conditions (37 °C, 24 h). Then, the length and width of the inhibition zone were measured with a slide rule. To calculate the area of the ZOI, we hypothesized that the shape of the ZOI was oval using the following equation Eq. (3):

$$ZOI\ area = \left(\frac{ZOI\ length}{2}\right) \times \left(\frac{ZOI\ width}{2}\right) \quad (3)$$

### 2.5 Statistical methods

Analysis was performed using the SAS 9.4 statistical software package. First, linear regression examining the relationship between different variables and the initial copper ion concentration was performed. Next, multiple linear regression analysis examining the relationship between the ZOI and variables of the samples was performed.

## 3 Results and discussion

### 3.1 Characterization of CS and CST composites

The SEM results are shown in Fig. 1. The surface morphology of CS was smoother than that of the CST composites, and the structure of CS was more porous than that of the CST composites. Comparing the textures of all samples, the CST composites had thicker structures than CS because of the presence of $TiO_2$ nanoparticles on the porous surface of CS. As the concentration of glutaraldehyde was increased, the porosity of the composite decreased, and their structure became more close-packed. EDS analysis of the CS and CST composites is shown in Figs. S3 and S4. Carbon (C), oxygen (O), and titanium (Ti) were clearly observed on the as-synthesized samples, which suggested the successful synthesis of CS and CST composites. Additionally, compositional analysis by EDS indicated that the relative concentration of carbon increased with respect to the glutaraldehyde concentration. According to Figs. S3 and S4, the Ti content of the CST-V composites (exchanged with ammonia solution) ranged from 32 to 38%. The Ti content of the CST-X composites (without exchange with ammonia solution) ranged from 19 to 22%. The exchange treatment with ammonia significantly increased the content of Ti in the CST composites. Ammonia solution endowed the CS surface with a porous structure. This might be caused by phase inversion because the excess acetic acid was neutralized by ammonia solution [21]. The possible reaction mechanism for the reaction between ammonia and CS or CST composites during synthesis is demonstrated in Fig. S5.

The physicochemical properties of the as-synthesized sample surfaces were determined by obtaining nitrogen adsorption-desorption isotherms with respect to the surface area and pore size distribution. The $N_2$ adsorption-desorption isotherms and corresponding pore size distribution curves of the as-synthesized samples are shown in Fig. 2a and b. The $S_{BET}$ and pore volume (Vpore) are shown in Table 1. The results showed that most of the samples presented a relationship among $S_{BET}$, the degree of crosslinking, and whether exchange occurred between the sample surface and ammonia solution. Figure 2c and d show that the proportion of cavities in the samples exchanging ammonia solution was greater than that of the others. Figure 2a and b show that the $N_2$ adsorption-desorption isotherms of the samples are separated by a different type. According to the International Union of Pure and Applied Chemistry classification system, the adsorption-desorption isotherms of CS are type IV, suggesting the existence of mesopores (pores with diameters between 2 and 50 nm), and the isotherms of the CST composites are type III, suggesting that they are not porous [22]. The samples with a higher crosslink yield and more contraction during ammonia solution treatment had a lower $S_{BET}$. This phenomenon can be seen in Table 1.

The structural changes of CS in the presence of $TiO_2$ were evaluated by FT-IR spectroscopy. Figure 3a and b show the spectra used to determine the chemical structure of the as-synthesized CS and CST samples. The

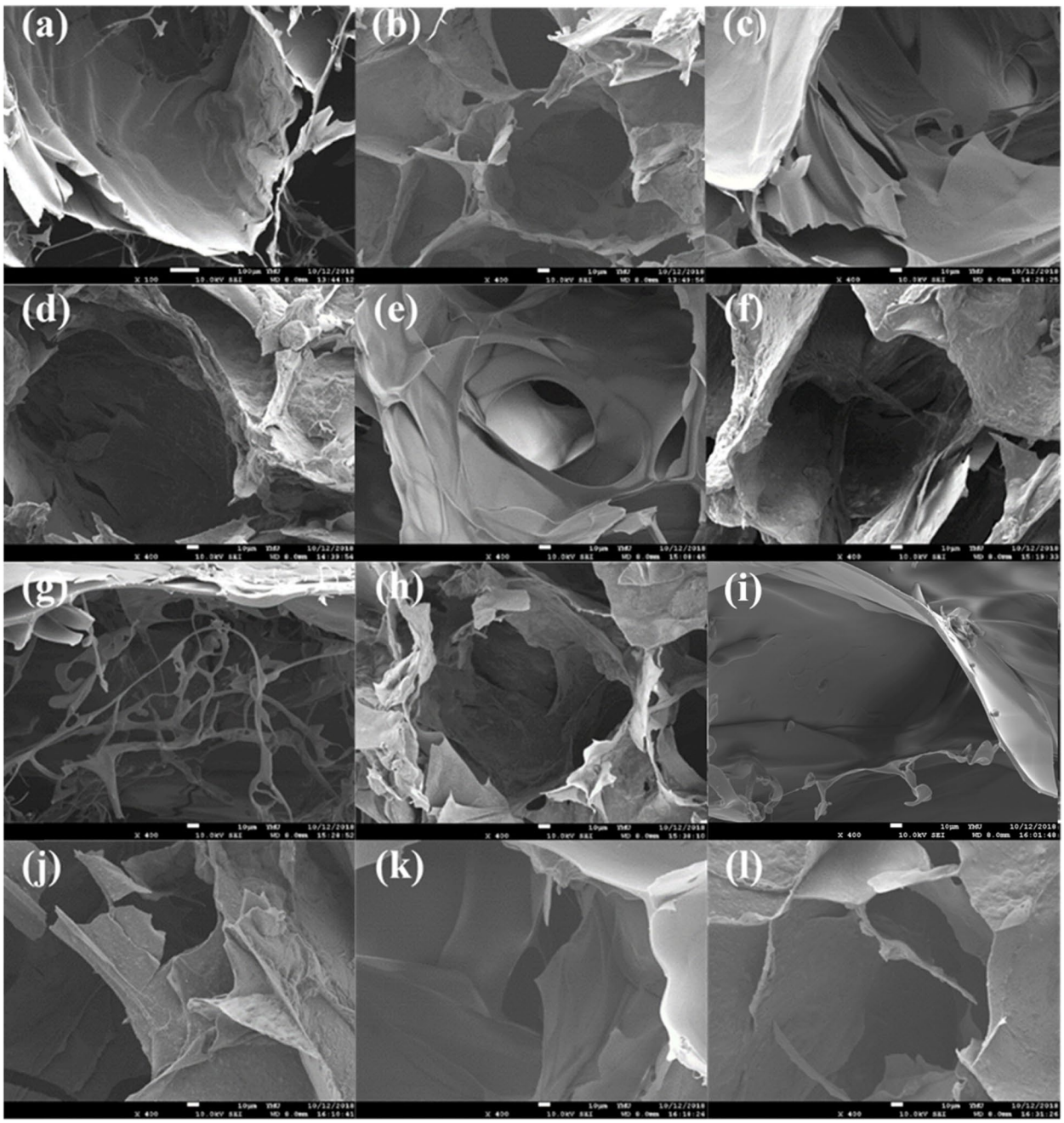


**Fig. 1** SEM images of the (**a**) 3%CS-V, (**b**) 3%CST-V, (**c**) 5%CS-V, (**d**) 5%CST-V, (**e**) 7%CS-V, (**f**) 7%CST-V, (**g**) 3%CS-X, (**h**) 3%CST-X, (**i**) 5%CS-X, (**j**) 5%CST-X, (**k**) 7%CS-X, and (**l**) 7%CST-X samples

deacetylated chitosan showed vibrations at approximately 1650 and 1560 $cm^{-1}$. These peaks were assigned to amide group I associated with C=O stretching vibrations and amide group II resulting from N-H bending vibrations. Additional $-CH_2$ bending peaks were observed at 1380 and 1324 $cm^{-1}$. The saccharide structure showed anti-symmetric stretching of the C–O–C bridge at 896 and 1158 $cm^{-1}$, and skeletal vibrations involving C–O stretching occurred at 1086 and 1028 $cm^{-1}$ [23–25]. The peaks at 2371 $cm^{-1}$ were typical of C-H stretching. The stronger intensity of the C-H stretching band at 2371 $cm^{-1}$ confirms the introduction of aliphatic chains from glutaraldehyde by crosslinking [26]. A wide strong band was shown at 3478 $cm^{-1}$

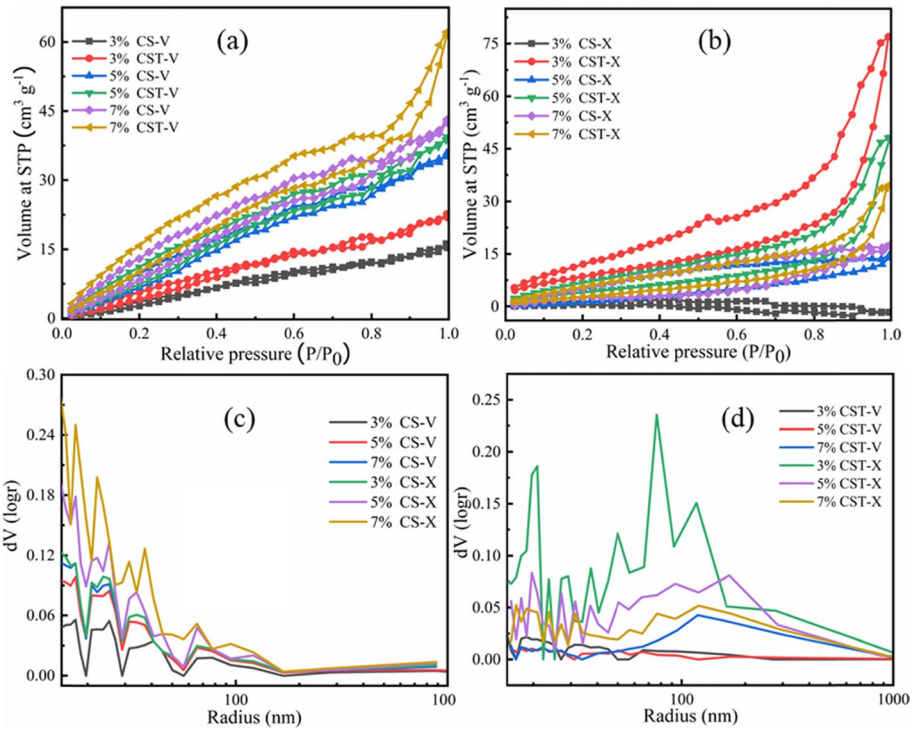


**Fig. 2** $N_2$ adsorption-desorption isotherms of the as-synthesized samples (**a**) with exchange with the ammonia solution and (**b**) without exchange with the ammonia solution. (**c**) pore size distribution curves of CS with and without exchange of ammonia solution and (**d**) pore size distribution curves of the CST composites with and without exchange of ammonia solution

**Table 1** BET surface area ($S_{BET}$) and pore volume ($V_{pore}$) of the as-synthesized samples

| Samples | $S_{BET}$ ($m^2 g^{-1}$)[a] | $V_{pore}$ ($cm^3 g^{-1}$)[b] |
|---|---|---|
| 3%CS-V | 30 | 0.026 |
| 3%CST-V | 10 | 0.011 |
| 5%CS-V | 28 | 0.019 |
| 5%CST-V | 5 | 0.006 |
| 7%CS-V | 29 | 0.034 |
| 7%CST-V | 9 | 0.028 |
| 3%CS-X | 2 | 0.010 |
| 3%CST-X | 40 | 0.12 |
| 5%CS-X | 24 | 0.017 |
| 5%CST-X | 22 | 0.071 |
| 7%CS-X | 21 | 0.035 |
| 7%CST-X | 18 | 0.049 |

[a] BET specific surface area; [b] Total pore volume measured at $P/P_0 = 0.99$

due to the stretching of OH, and this band overlapped the band attributed to the N-H stretching of amide [27]. The peak at 1400 $cm^{-1}$ is attributed to C-H bending vibrations in the $CH_2$ group, and the typical peak at 1339 $cm^{-1}$ is attributed to C-H bending vibrations in the $CH_3$ group [28].

The peaks at 1636 and 662 $cm^{-1}$ were attributed to H-O-H bending and Ti-O-Ti stretching vibrations, respectively, which are typical characteristics of $TiO_2$ [29, 30]. In Fig. 3b, the FT-IR spectrum of CST crosslinking with glutaraldehyde showed an increase in the intensity of the amide group peak, which might have resulted from the interaction of $Ti^{+4}$ with the amide group of chitosan [31]. In this study, $TiO_2$ signals were not observed from approximately 400 to 662 $cm^{-1}$. Ali et al. [32] reported similar patterns on pure CS and CS@$TiO_2$ nanocomposites in their FT-IR spectra. Therefore, it was suggested that $TiO_2$ existed on the surface of chitosan without affecting its chemical structures.

The thermal stability of CS and CST composites was assessed through Differential Scanning Calorimetry/TGA studies. Figure 4 shows the thermal stability and degree of crosslinking of the as-synthesized samples. As shown in previous studies, the weight losses below 100 °C were attributed to the desorption of water. Conspicuous weight losses from 180 to 400 °C were observed as the thermal degradation of CS progressed; notably, the introduction of a crosslinked structure was supposed to enhance thermal stability [33, 34]. In our results, noticeable weight losses appeared from 170 to

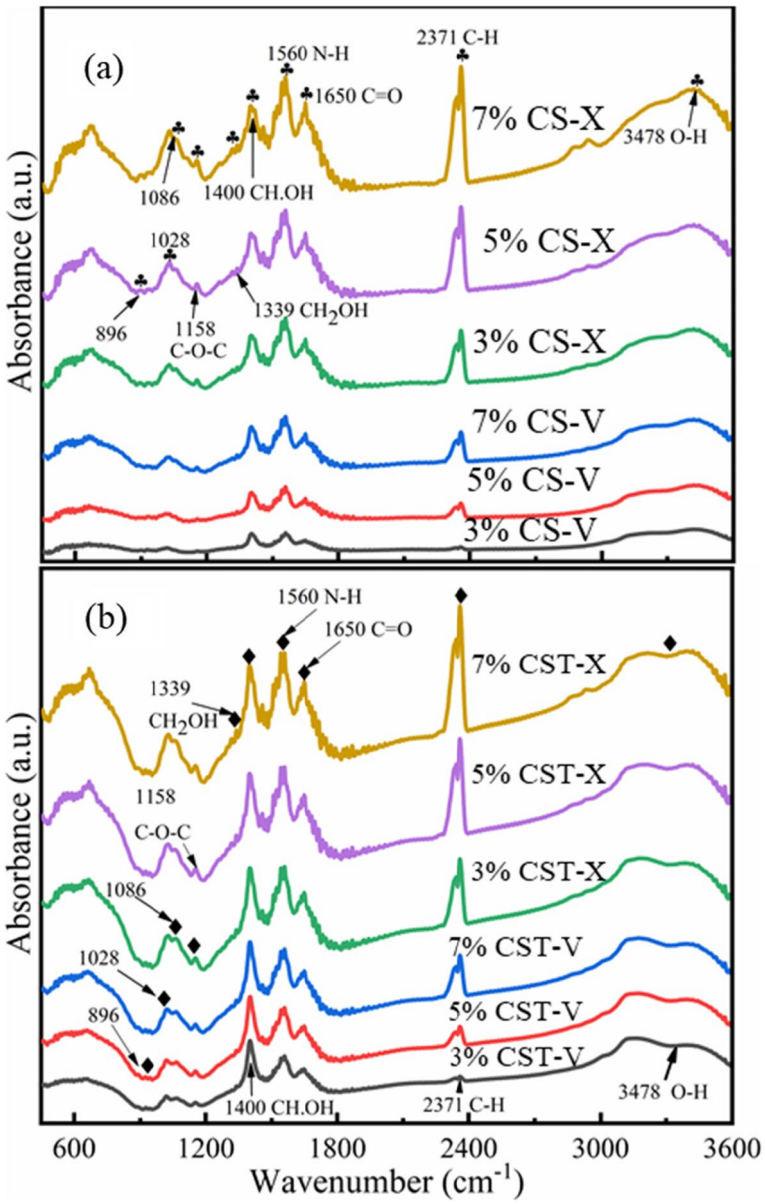


**Fig. 3** FTIR spectra of (**a**) CS and (**b**) CST composites

400 °C, as shown in other studies. The apparent weight of the residues of CST may indicate the containment of $TiO_2$; the 3%CST-X sample was more thermostable than other samples. This behavior was attributed to the presence of $TiO_2$. The weight loss percentage is proportional to the degree of crosslinking, with a higher glutaraldehyde concentration having higher thermal stability.

Figure S6 shows the slope of thermal stability, and the peak at 100 °C was attributed to the desorption of water. The other peaks at approximately 255 and 510 °C were attributed to the pyrolysis of materials, and the peaks of CS and the CST composites were similar. This result suggested that pyrolysis at 255 and 510 °C was CS pyrolysis.

### 3.2 Adsorption mechanism

The adsorption capacities of all samples are shown in Table S1. Among the four different initial concentrations, most of the samples had a better adsorption capacity when the initial concentration was 300 ppm. Two-thirds of the samples showed an improved adsorption effect after exchange with the ammonia solution;

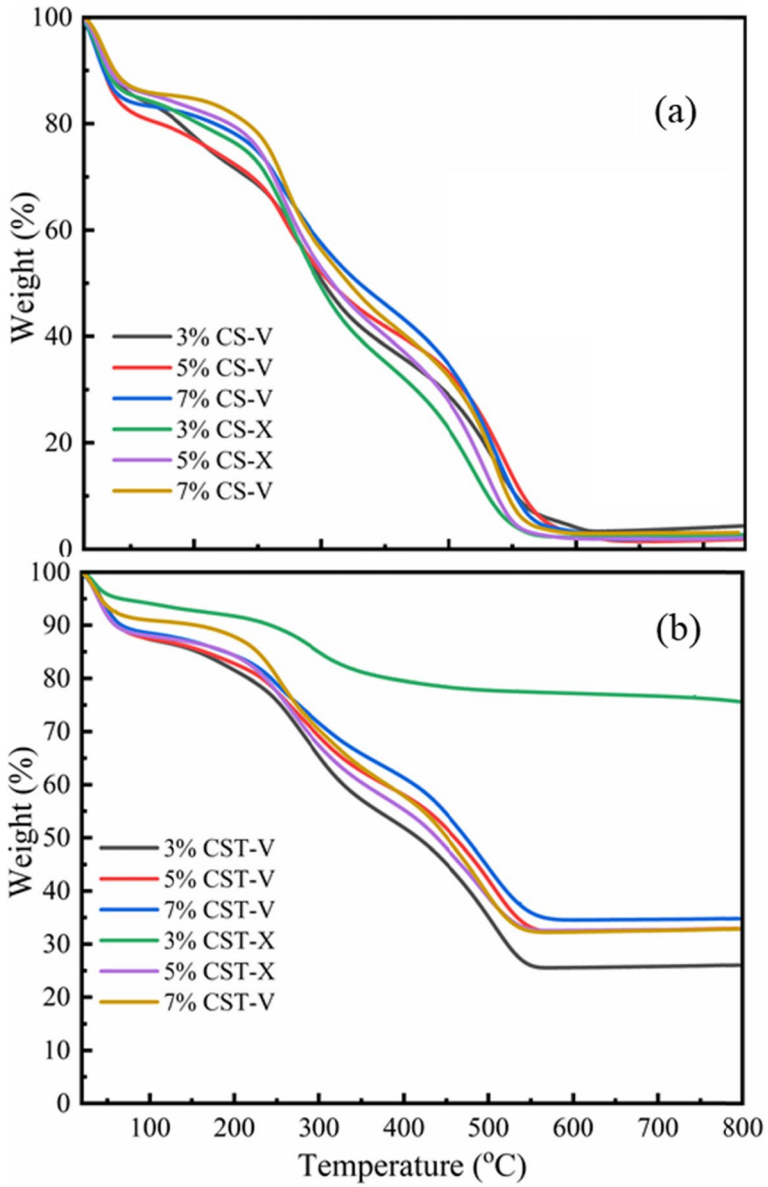


**Fig. 4** TGA curves of (**a**) CS and (**b**) CST composites

for instance, the 3%CS, 5%CS, 5%CST, and 7%CST samples after the exchange treatment had better adsorption capability. The addition of $TiO_2$ had a positive effect on Cu adsorption, and most of the CS samples with $TiO_2$ composites had better effectiveness. Freundlich isotherm models were used to fit the isotherms of the CS and CST composite samples. The fitting curves of the Freundlich isotherm models are shown in Fig. 5. The magnitude of $K_F$ is a relative measure of adsorption capacity. The constant n is a parameter related to the intensity of adsorption, which varies with the heterogeneity of the adsorbent. According to Thommes et al. and Mishra and Patel [22, 35], for favorable adsorption, the $n$ values should be in the range of 1–10. Statistical analysis based on the effect of the initial $Cu^{2+}$ concentration in solution on the adsorption capacity ($q_e$) is shown in Table 2. The $p$-value of the degree of crosslinking (3, 5, 7%) and initial $Cu^{2+}$ concentration was lower than 0.001. Thus, the degree of crosslinking and initial $Cu^{2+}$ concentration can also affect $q_e$. Glutaraldehyde crosslinks the amino and hydroxyl groups of chitosan. A lower crosslinking degree has a positive impact on the effectiveness

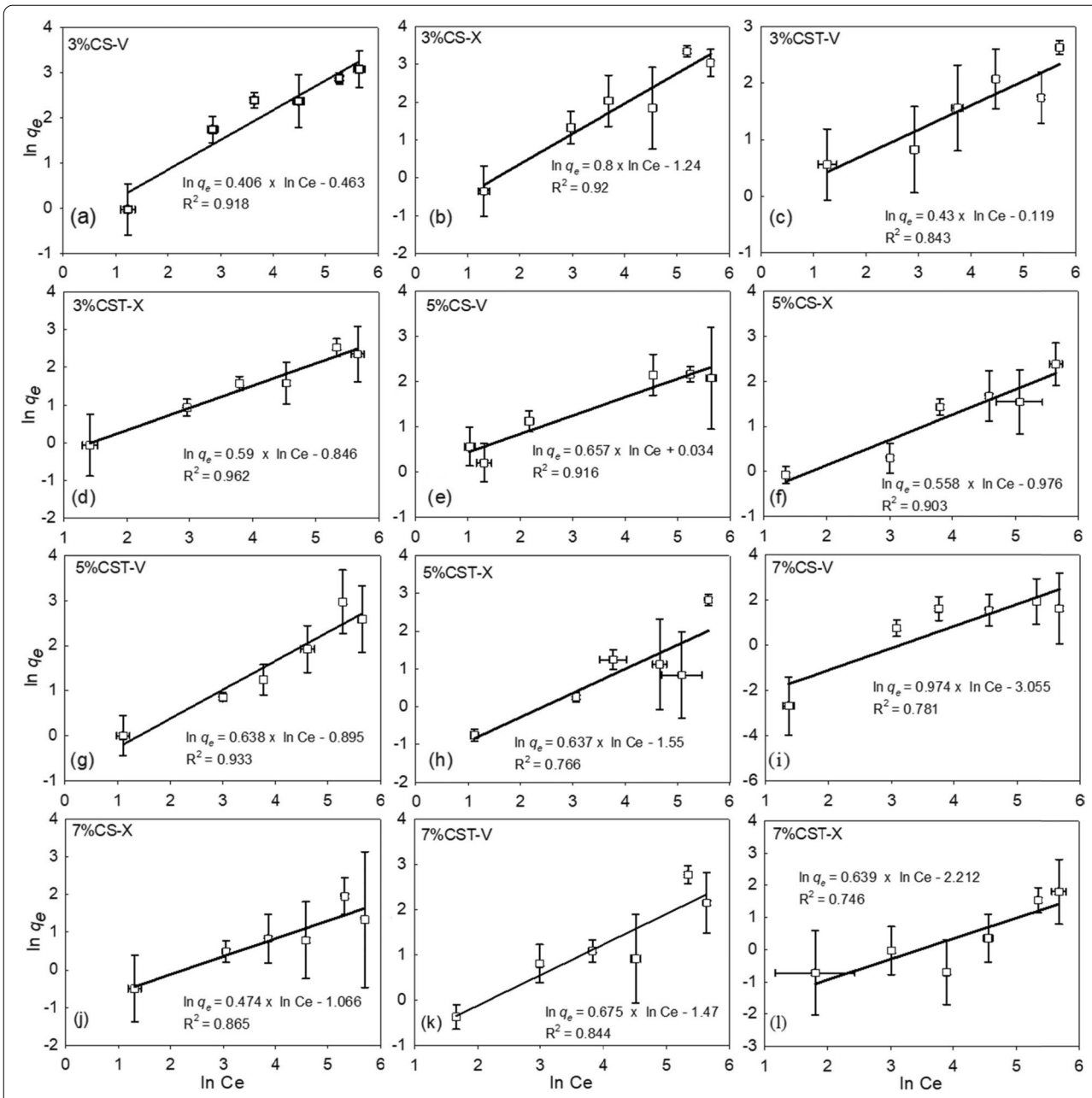


**Fig. 5** Fitting curves of the Freundlich isotherm models for the adsorption of copper ions in aqueous solution on (**a**) 3%CS-V, (**b**) 3%CS-X, (**c**) 3%CST-V, (**d**) 3%CST-X, (**e**) 5%CS-V, (**f**) 5%CS-X, (**g**) 5%CST-V, (**h**) 5%CST-X, (**i**) 7%CS-V, (**j**) 7%CS-X, (**k**) 7%CST-V, and (**l**) 7%CST-X; error bars represent standard deviations of triplicate runs ($n = 3$)

of copper ion adsorption without causing a significant decrease in adsorption capacity. This is because relatively abundant amino and hydroxyl groups existed on the chitosan network structure. However, a higher concentration of glutaraldehyde blocks amine groups, which can limit the sorption capacity of the sorbent. The amine ($-NH_2$) groups [FTIR peaks at 1560 and 3478 $cm^{-1}$ (overlap with the stretching of –OH groups)] on CS chains serve as coordination sites, thereby playing an important role in the adsorption capacity and stability of CS because $NH_2$ groups in CS work as copper adsorption sites [28]. Therefore, we chose the composite with the best adsorption capacity (3%CS-V, 300 ppm $Cu^{2+}$) to test the effect of the initial pH value of the solution on Cu adsorption;

**Table 2** Effect of the initial $Cu^{2+}$ concentration in solution on the equilibrium adsorption capacity ($q_e$)

| Variable | B | 95% CI | | *p*-value |
|---|---|---|---|---|
| Adding $TiO_2$ | -2 | −3.70 | −0.62 | 0.006* |
| Exchange with ammonia solution | 1 | −0.08 | 2.90 | 0.065 |
| Crosslinking degree (3, 5, 7%) | −1 | −1.80 | −0.91 | < 0.001** |
| $S_{BET}$ | −0.08 | −0.15 | −0.01 | 0.035 |
| Initial $Cu^{2+}$ concentration | 0.05 | 0.05 | 0.06 | < 0.001** |

*B* estimated factor, *CI* confidence interval, *statistically significant, ** highly statistically significant

the result is shown in Fig. 6. At low pH values from 1 to 3, the adsorption of Cu on the CST composite was relatively low because CS was unstable and tended to solubilize, and the acrylate groups were protonated. This makes the composites unable to form complexes with $Cu^{2+}$. The highest absorption capacity occurs at pH 4.5 on the CST composite because more carboxylate groups are ionized, which results in an increase in the affinity for copper cations via electrostatic interactions. Grande-Tovar et al. [27] reported a similar finding; the highest adsorption capacities for copper and lead ions were obtained at pH 4 on CS@grafted-polyacrylic acid.

### 3.3 Antimicrobial efficacy

After the adsorption test, the best condition (300 ppm $Cu^{2+}$) was chosen to perform the antimicrobial experiments using a ZOI assay to examine the antimicrobial efficacy, as shown in Figs. 7 and 8. The average width and area are shown in Table S2, and linear regression examining the relationship between the area of the ZOI and other variables divided bacteria into two kinds, as listed in Table 3. In the linear regression study, we set the degree of crosslinking and initial $Cu^{2+}$ concentration as categorical variables. First, the results against *E. coli* in Table 3 showed that both the addition of $TiO_2$ and exchange with ammonia solution had negative directivity. These two treatments decreased the porosity and adsorption capability of the composites, which led to a decrease in their antimicrobial efficiency. The estimated factor (B) of the initial $Cu^{2+}$ concentration was high, which indicated that a higher initial concentration of $Cu^{2+}$ could enhance the antimicrobial efficiency. According to Table 3, the antimicrobial efficacy was affected by copper ions more than $TiO_2$ addition and glutaraldehyde concentration. In addition, in accordance with the estimated factor, B (negative means antimicrobial effect compared to the reference group), and *p*-value (< 0.01* means statistically significant) in Table 3, $TiO_2$ addition and exchange with ammonia solution had a more significant effect on the antimicrobial efficiency against *S. epidermidis* [Gram+, $TiO_2$ addition, B = − 33, *p*-value < 0.001; exchange with ammonia solution, B = − 38, *p*-value < 0.001] than against *E. coli* [Gram-, $TiO_2$ addition, B = − 5, *p*-value = 0.771; exchange with ammonia solution, B = − 1, *p*-value = 0.948]. Perelshtein et al. [36] also found that crystalline $TiO_2$ nanoparticles demonstrated a more significant antimicrobial effect on *S. aureus* (Gram+) than *E. coli* (Gram-) under visible light, which is relevant to carotenoids (a yellow pigment produced by *S. aureus*) acting as photosensitizers

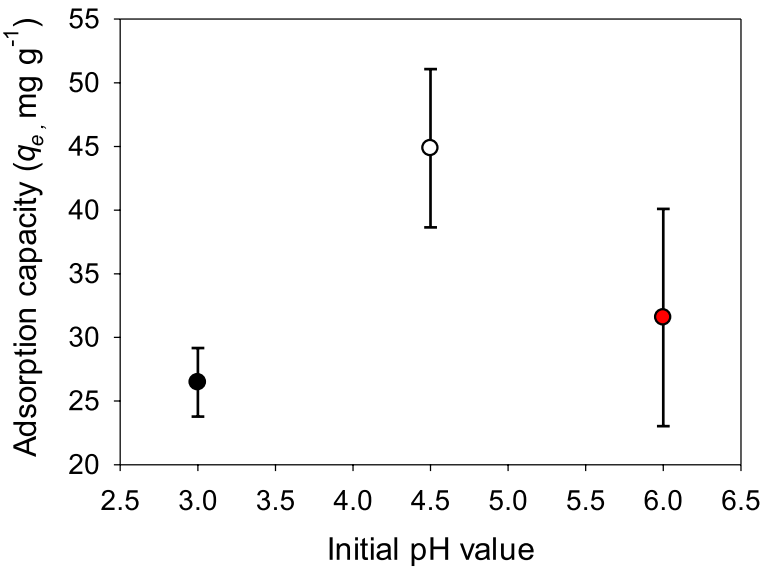


**Fig. 6** Effect of solution's initial pH value on adsorption capacity ($q_e$); error bars represent standard deviations of triplicate experiments ($n = 3$)

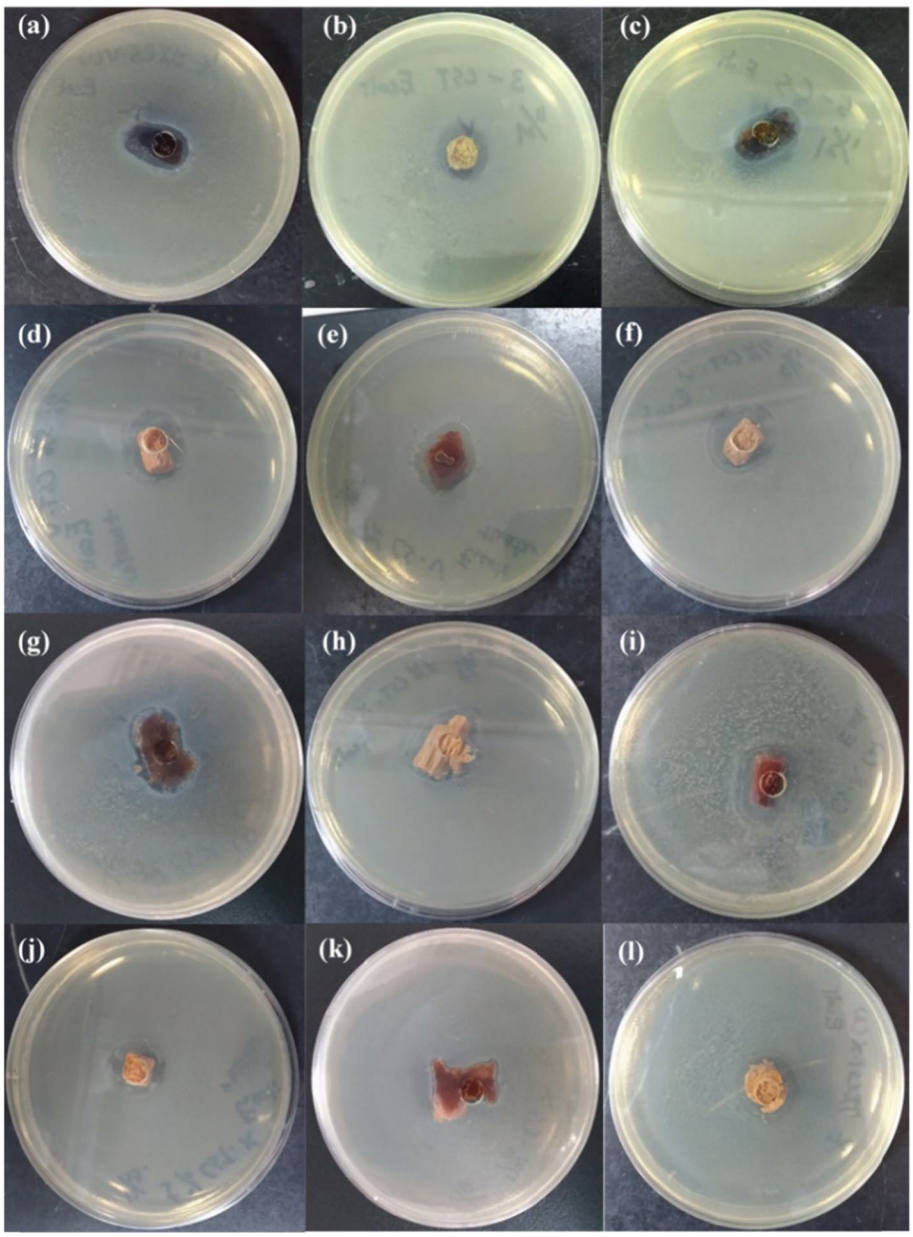


**Fig. 7** Zone of inhibition of (**a**) 3%CS-V, (**b**) 3%CST-V, (**c**) 5%CS-V, (**d**) 5%CST-V, (**e**) 7%CS-V, (**f**) 7%CST-V, (**g**) 3%CS-X, (**h**) 3%CST-X, (**i**) 5%CS-X, (**j**) 5%CST-X, (**k**) 7%CS-X, and (**l**) 7%CST-X against *E. coli* growth

for $TiO_2$ photocatalysis. *S. epidermidis* also produces white pigments of a xanthophyllic nature [37], and these pigments may also act as photosensitizers for $TiO_2$ photocatalysis. In addition, the exchange treatment with ammonia significantly increased the Ti content of the CST composites (see Section 3.1, Figs. S3 and S4). This treatment enhanced the antimicrobial efficiency of CST composites against *S. epidermidis.*

Similarly, we used untreated wastewater from a PCB factory to conduct experiments with the composite samples with the best adsorption capability (3%CS-V) and the best antibacterial efficiency (7%CST-V). The ZOI results of the industrial wastewater without dilution and after 50-fold dilution are shown in Fig. 9, Tables S3, S4 and S5, revealing excellent antimicrobial efficiency against *S. epidermidis and E. coli*.

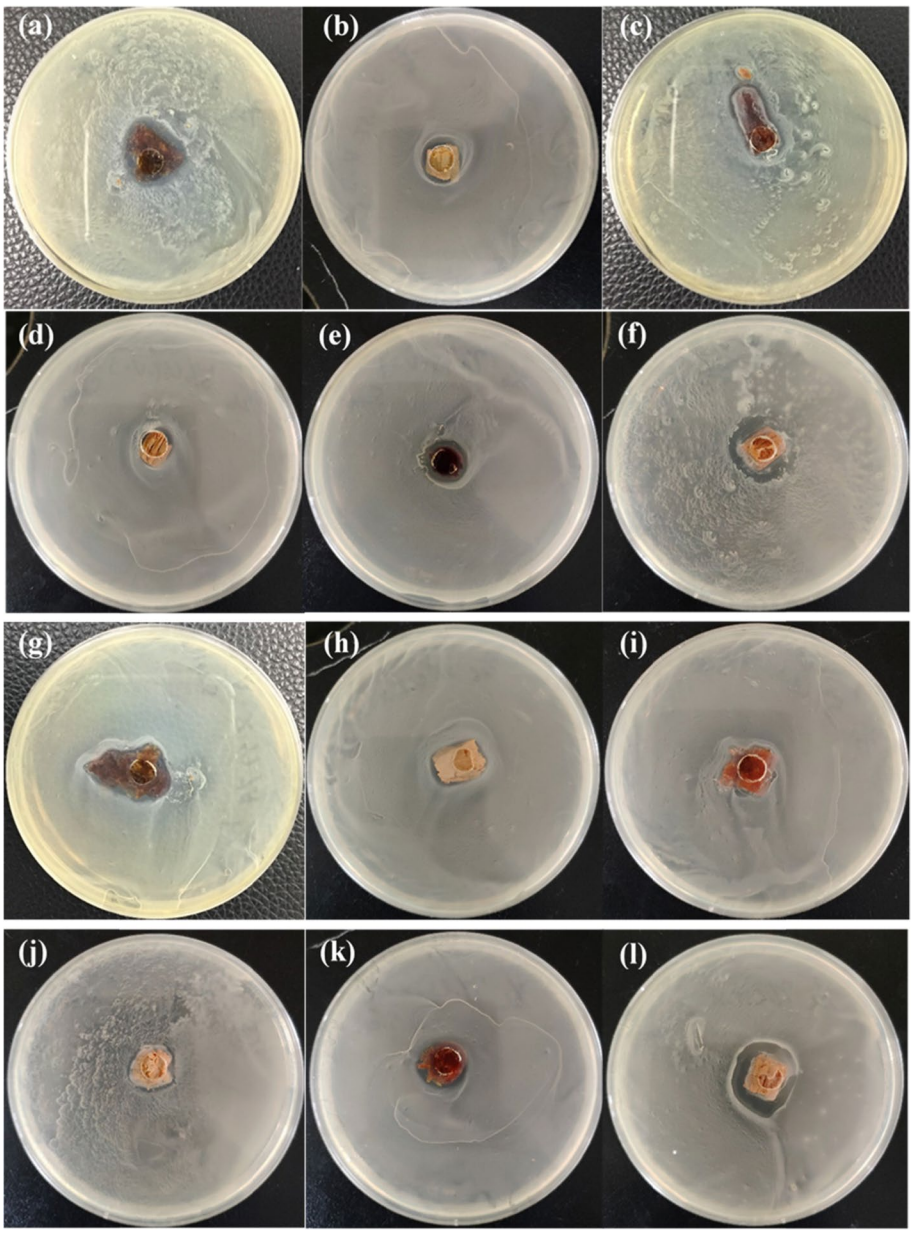


**Fig. 8** Zone of inhibition of (**a**) 3%CS-V, (**b**) 3%CST-V, (**c**) 5%CS-V, (**d**) 5%CST-V, (**e**) 7%CS-V, (**f**) 7%CST-V, (**g**) 3%CS-X, (**h**) 3%CST-X, (**i**) 5%CS-X, (**j**) 5%CST-X, (**k**) 7%CS-X, and (**l**) 7%CST-X against *S. epidermidis* growth

## 4 Conclusions

In this work, we synthesized CS and CST composites with different concentrations of glutaraldehyde solution by a simple method involving a crosslinking process and freeze-drying technique. There were some notable characteristics of the as-synthesized samples: the weight percentage of carbon increased with respect to the concentration of glutaraldehyde, and the samples with a higher crosslink yield and more contraction during ammonia solution exchange resulted in a lower $S_{BET}$. Among the as-synthesized samples, 3%CS-V with an initial concentration of 300 ppm exhibited a preferable adsorption capacity for copper ions, and the maximum adsorption capacity was 31 mg $g^{-1}$. The Freundlich model fits the adsorption isotherms better than the Langmuir model.

The results revealed the shape, surface, size, and elements of the material, and the study confirmed

**Table 3** Regression analysis of the effect of the inhibition zone on other variables

| Test species | *E. coli* (*N* = 83) | | | | *S. epidermidis* (*N* = 90) | | | |
|---|---|---|---|---|---|---|---|---|
| **Variable** | **B** | **95% CI** | | ***p*-value** | **B** | **95% CI** | | ***p*-value** |
| Adding $TiO_2$ | −5 | −38 | 29 | 0.771 | −36 | −52 | −20 | < 0.001** |
| Without adding $TiO_2$ | 0 | | | | 0 | | | . |
| Exchange with ammonia solution | −1 | −35 | 32 | 0.948 | −38 | −54 | −23 | < 0.001** |
| Without exchange with ammonia solution | 0 | | | | 0 | | | |
| Crosslinking degree (3%) | 0 | | | | 0 | | | |
| Crosslinking degree (5%) | −45 | −86 | −4 | 0.033* | −35 | −54 | −16 | < 0.001** |
| Crosslinking degree (7%) | −22 | −65 | 22 | 0.331 | −27 | −47 | −7 | 0.009* |
| Adsorption capacity | 0.2 | −2 | 2 | 0.799 | 0.34 | −0.75 | 1 | 0.540 |
| Initial $Cu^{2+}$ concentration (100 ppm) | 0 | | | | 0 | | | |
| Initial $Cu^{2+}$ concentration (300 ppm) | 79 | 39 | 120 | < 0.001** | 12 | −5 | 30 | 0.177 |

*B* estimated factor, *CI* confidence interval, * statistically significant, ** highly statistically significant

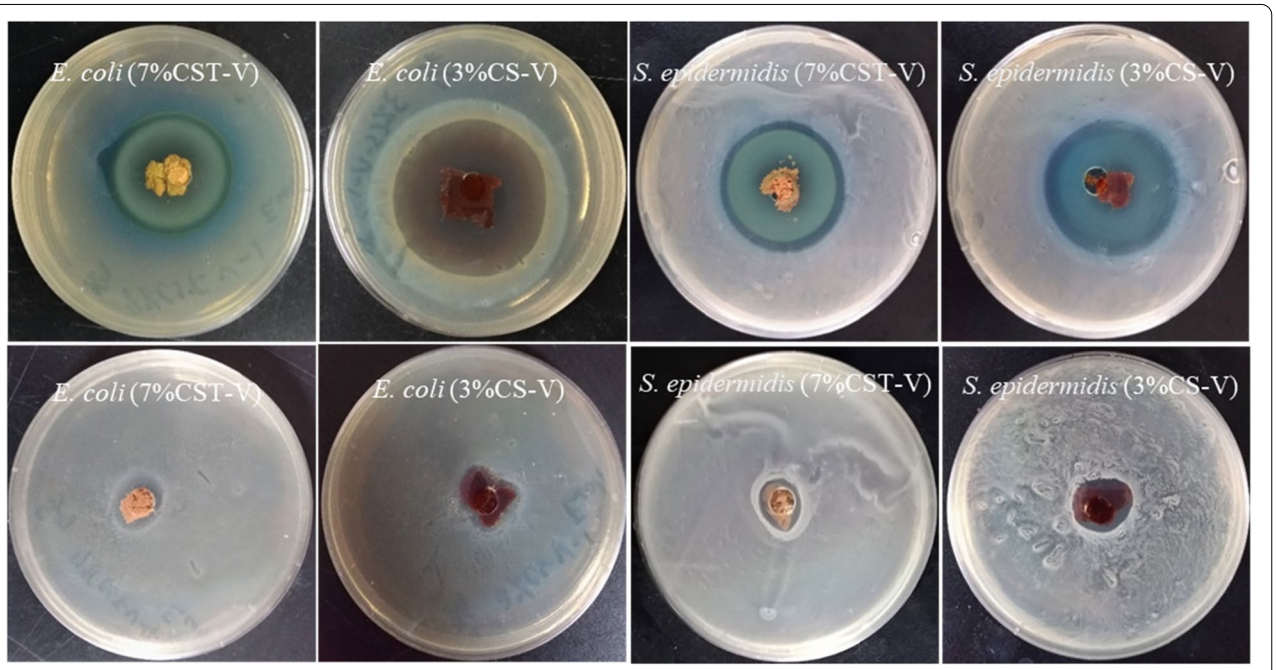


**Fig. 9** ZOI with the best $q_e$ (3%CS-V) and antimicrobial efficacy (7% CST-V) for inhibition of the growth of *E. coli* and *S. epidermidis*. (The upper rows show the materials that adsorbed wastewater without treatment, and the lower rows show the materials that adsorbed wastewater diluted 50 times)

the effect of Cu adsorption and its ability to inhibit *E. coli*. The estimated factor in the initial $Cu^{2+}$ concentration was high, indicating that a higher initial $Cu^{2+}$ concentration enhanced the antimicrobial efficiency of the material. Furthermore, the copper ions affected the antimicrobial efficacy against *E. coli* more than $TiO_2$ addition and glutaraldehyde concentration. The addition of $TiO_2$ and exchange with ammonia solution had a more significant effect on the antimicrobial efficiency against *S. epidermidis* than against *E. coli*.

## Supplementary Information

The online version contains supplementary material available at https://doi.org/10.1186/s42834-022-00138-7.

**Additional file 1.**

**Acknowledgments**
This work was supported by the Ministry of Science and Technology of Taiwan (MOST 109-2621-M-010-002). The authors are grateful to the Electron Microscopy Facility at National Yang Ming Chiao Tung University for providing the TEM, SEM and EDS images. We also appreciate the BET and BJH data obtained from the facility of National Chung Hsing University.

**Authors' contributions**
Chien Su and Abiyu Kerebo Berekute conducted the experiments, wrote the study and contributed equally. Kuo-Pin Yu is Chien Su and Abiyu Kerebo Berekute's advisor. He provided research ideas and guidance for this study. All authors read and approved the final manuscript.

**Funding**
This work was supported by the Ministry of Science and Technology of Taiwan (MOST 108–2621-M-010-002).

**Availability of data and materials**
All data generated or analyzed during this study are available within the article and its supplementary materials.

## Declarations

**Competing interests**
The authors declare they have no competing interests.

**Author details**
[1]Institute of Environmental and Occupational Health Sciences, National Yang Ming Chiao Tung University, Taipei 112304, Taiwan. [2]International Ph.D. Program in Environmental Science and Technology, National Yang Ming Chiao Tung University, Taipei 112304, Taiwan.

Received: 21 July 2021 Accepted: 24 April 2022
Published online: 08 May 2022

**References**

1. Chen L, Hao HY, Zhang WT, Shao ZQ. Adsorption mechanism of copper ions in aqueous solution by chitosan-carboxymethyl starch composites. J Appl Polym Sci. 2020;137:48636.
2. Ali H, Khan E, Ilahi I. Environmental chemistry and ecotoxicology of hazardous heavy metals: environmental persistence, toxicity, and bioaccumulation. J Chem-NY. 2019;2019:6730305.
3. Shi YY, Zhang QH, Feng LD, Xiong QP, Chen J. Preparation and adsorption characters of Cu(II)-imprinted chitosan/attapulgite polymer. Korean J Chem Eng. 2014;31:821–7.
4. Patino-Ruiz DA, De Avila G, Alarcon-Suesca C, Gonzalez-Delgado AD, Herrera A. Ionic cross-linking fabrication of chitosan-based beads modified with FeO and $TiO_2$ nanoparticles: adsorption mechanism toward naphthalene removal in seawater from Cartagena Bay area. ACS Omega. 2020;5:26463–75.
5. El Kadib A, Molvinger K, Guimon C, Quignard F, Brunel D. Design of stable nanoporous hybrid chitosan/titania as cooperative bifunctional catalysts. Chem Mater. 2008;20:2198–204.
6. Nilsen-Nygaard J, Strand SP, Varum KM, Draget KI, Nordgard CT. Chitosan: gels and interfacial properties. Polymers-Basel. 2015;7:552–79.
7. Chen YW, Wang JL. Preparation and characterization of magnetic chitosan nanoparticles and its application for Cu(II) removal. Chem Eng J. 2011;168:286–92.
8. Yuan LL, Yao QD, Liang YX, Dan Y, Wang YX, Wen HT, et al. Chitosan based antibacterial composite materials for leather industry: a review. J Leather Sci Eng. 2021;3:12.
9. Al-Sherbini ASA, Ghannam HEA, El-Ghanam GMA, El-Ella AA, Youssef AM. Utilization of chitosan/Ag bionanocomposites as eco-friendly photocatalytic reactor for bactericidal effect and heavy metals removal. Heliyon. 2019;5:e01980.
10. Wang JW, Kuo YM. Preparation and adsorption properties of chitosan-poly(acrylic acid) nanoparticles for the removal of nickel ions. J Appl Polym Sci. 2008;107:2333–42.
11. Peralta ME, Nistico R, Franzoso F, Magnacca G, Fernandez L, Parolo ME, et al Highly efficient removal of heavy metals from waters by magnetic chitosan-based composite. Adsorption. 2019;25:1337–47.
12. Goy RC, de Britto D, Assis OBG. A review of the antimicrobial activity of chitosan. Polimeros. 2009;19:241–7.
13. Fan XL, Chen KK, He XC, Li N, Huang JB, Tang KY, et al. Nano-$TiO_2$/collagen-chitosan porous scaffold for wound repairing. Int J Biol Macromol. 2016;91:15–22.
14. Foster HA, Ditta IB, Varghese S, Steele A. Photocatalytic disinfection using titanium dioxide: spectrum and mechanism of antimicrobial activity. Appl Microbiol Biot. 2011;90:1847–68.
15. Maness PC, Smolinski S, Blake DM, Huang Z, Wolfrum EJ, Jacoby WA. Bactericidal activity of photocatalytic $TiO_2$ reaction: toward an understanding of its killing mechanism. Appl Environ Microb. 1999;65:4094–8.
16. Zhao GJ, Stevens SE. Multiple parameters for the comprehensive evaluation of the susceptibility of *Escherichia coli* to the silver ion. BioMetals. 1998;11:27–32.
17. Koyama Y, Taniguchi A. studies on chitin X. Homogeneous cross-linking of chitosan for enhanced cupric ion adsorption. J Appl Polym Sci. 1986;31:1951–4.
18. Hill SD, Berry CW, Seale NS, Kaga M. Comparison of antimicrobial and cytotoxic effects of glutaraldehyde and formocresol. Oral Surg Oral Med O. 1991;71:89–95.
19. Li A, Lin RJ, Lin C, He BY, Zheng TT, Lu LB, et al. An environment-friendly and multi-functional absorbent from chitosan for organic pollutants and heavy metal ion. Carbohyd Polym. 2016;148:272–80.
20. Carp O, Huisman CL, Reller A. Photoinduced reactivity of titanium dioxide. Prog Solid State Ch. 2004;32:33–177.
21. Xu XY, Dong PJ, Feng Y, Li F, Yu HJ. A simple strategy for preparation of spherical silica-supported porous chitosan matrix based on sol-gel reaction and simple treatment with ammonia solution. Anal Methods-UK. 2010;2:546–51.
22. Thommes M, Kaneko K, Neimark AV, Olivier JP, Rodriguez-Reinoso F, Rouquerol J, et al. Physisorption of gases, with special reference to the evaluation of surface area and pore size distribution (IUPAC Technical Report). Pure Appl Chem. 2015;87:1051–69.
23. Smitha B, Sridhar S, Khan AA. Chitosan-sodium alginate polyion complexes as fuel cell membranes. Eur Polym J. 2005;41:1859–66.
24. Lawrie G, Keen I, Drew B, Chandler-Temple A, Rintoul L, Fredericks P, et al. Interactions between alginate and chitosan biopolymers characterized using FTIR and XPS. Biomacromolecules. 2007;8:2533–41.
25. Cordero-Arias L, Cabanas-Polo S, Gao HX, Gilabert J, Sanchez E, Roether JA, et al. Electrophoretic deposition of nanostructured-$TiO_2$/chitosan composite coatings on stainless steel. RSC Adv. 2013;3:11247–54.
26. Li Y, Qiu TB, Xu XY. Preparation of lead-ion imprinted crosslinked electrospun chitosan nanofiber mats and application in lead ions removal from aqueous solutions. Eur Polym J. 2013;49:1487–94.
27. Grande-Tovar CD, Vallejo W, Zuluaga F. Equilibrium and kinetic study of lead and copper ion adsorption on chitosan-grafted-polyacrylic acid synthesized by surface initiated atomic transfer polymerization. Molecules. 2018;23:2218.
28. Yadi MG, Benguella B, Gaouar-Benyelles N, Tizaoui K. Adsorption of ammonia from wastewater using low-cost bentonite/chitosan beads. Desalin Water Treat. 2016;57:21444–54.
29. Zhang H, Lv XJ, Li YM, Wang Y, Li JH. P25-graphene composite as a high performance photocatalyst. ACS Nano. 2010;4:380–6.
30. Dvoranova D, Brezova V, Mazur M, Malati MA. Investigations of metal-doped titanium dioxide photocatalysts. Appl Catal B-Environ. 2002;37:91–105.
31. Deveci I, Dogac YI, Teke M, Mercimek B. Synthesis and Characterization of chitosan/$TiO_2$ composite beads for improving stability of porcine pancreatic lipase. Appl Biochem Biotech. 2015;175:1052–68.
32. Ali F, Khan SB, Kamal T, Alamry KA, Asiri AM. Chitosan-titanium oxide fibers supported zero-valent nanoparticles: highly efficient and easily retrievable catalyst for the removal of organic pollutants. Sci Rep-UK. 2018;8:6260.
33. Neto CGT, Giacometti JA, Job AE, Ferreira FC, Fonseca JLC, Pereira MR. Thermal analysis of chitosan based networks. Carbohyd Polym. 2005;62:97–103.
34. Zeng LT, Qin CQ, Wang LS, Li W. Volatile compounds formed from the pyrolysis of chitosan. Carbohyd Polym. 2011;83:1553–7.
35. Mishra PC, Patel RK. Removal of lead and zinc ions from water by low cost adsorbents. J Hazard Mater. 2009;168:319–25.

36. Perelshtein I, Applerot G, Perkas N, Grinblat J, Gedanken A. A one-step process for the antimicrobial finishing of textiles with crystalline $TiO_2$ nanoparticles. Chem-Eur J. 2012;18:4575–82.
37. Sandvik O, Brown RW. Spectrophotometric characterization of pigments produced by *Staphylococcus epidermidis* strains isolated from bovine udders. J Bacteriol. 1965;89:1201–8.

## Publisher's Note

Springer Nature remains neutral with regard to jurisdictional claims in published maps and institutional affiliations.

**Ready to submit your research? Choose BMC and benefit from:**

- fast, convenient online submission
- thorough peer review by experienced researchers in your field
- rapid publication on acceptance
- support for research data, including large and complex data types
- gold Open Access which fosters wider collaboration and increased citations
- maximum visibility for your research: over 100M website views per year

**At BMC, research is always in progress.**

**Learn more** biomedcentral.com/submissions

BMC